EnABLES

EnABLES (Project no. 730957)

"European Infrastructure Powering the Internet of Things"

Deliverable 5.5

"Final report on simulation tools"

Dissemination level: PU

Responsible Beneficiary
U-BOLOGNA

Due Date
31st December 2021

Submission Date
30th March 2022

HORIZON 2020

H2020-INFRAIA-02-2017 – Integrating Activities for Starting Communities

EnABLES (Grant agreement 730957)

Integrating and Opening Existing National and Regional Research Infrastructures of European Interest

Summary					
No and name	**D5.5 – Final Report on Simulation Tools**[1]				
Status	Released	**Due**	Month 48	**Date**	31-Dec-2021
Author(s)	Aldo Romani, Cinzia Tamburini, Eleonora Franchi Scarselli, Luca Perilli, Francesco Cottone, Michael Hayes, Ben Breitung				
Editor	Aldo Romani				
Internal reviewers	Mario Konijnenburg, Claudio Gerbaldi				
DoW	Report on simulation tools and models related to energy consumption and generation in energy harvesting systems				
Dissemination Level	**PU – Public**				
Nature	Report				

Document history			
V	**Date**	**Author**	**Description**
Draft	22-Dec-2021	Aldo Romani	Draft and template of the main document
0.9	25-Jan-2022	Francesco Cottone, Ben Breitung, Michael Hayes, Eleonora Franchi Scarselli, Luca Perilli, Cinzia Tamburini, Aldo Romani	Feedback and additional contents from project partners
0.99	20-Mar-2022	-	Final draft completed and sent for internal review
1.0	28-Mar-2022	-	Final version
1.01	30-Mar-2022	-	Fixed minor issues and typos

1 **Disclaimer -** The information in this document is provided as is and no guarantee or warranty is given that the information is fit for any particular purpose. The user thereof uses the information at its sole risk and liability.

1 Table of Contents

2 Publishable Summary

Energy modelling is necessary at different stages in the design of Internet-of-Things (IoT) applications and for a variety of different types of devices and objects, ranging from single components to connected systems.

In order to assess the available input energy in a self-powered application, reliable modelling of energy transducers based on characterisation of commercial parts is necessary, along with simulation tools capable of combining realistic inputs with power conversion and application electronics. A technique for parameter identification of vibrational energy transducer is presented along with complementary web-based simulation tools for early energy predictions.

Besides characterisation of individual parts, system-level modelling is also fundamental to ensure the success of an IoT applications, in terms of battery life, energy autonomy when self-powered, and overall sustainability. Progresses in online simulation tools at system-level along with energy models for WSANs are presented and show the capability of designing and modulating the behavior of the corresponding IoT applications.

Since energy storage plays a key role, innovative components compatible with IoT trends have been developed by focusing on flexible energy storage systems and their characterization. Novel materials for energy storage devices are developed, along with ink-jet printing methods, since additive manufacturing techniques enable a stepwise manufacturing approach, allow the utilization of a broad range of different materials, and reduce waste production. Characterization is performed, and the obtained data can provide a basis for future calculations of more comple devices.

All energy aspects at different levels need to be considered to implement effective and sustainable IoT applications.

3 Introduction

Energy modelling is an utmost important topic for an effective deployment and exploitation of energy autonomous systems based on energy harvesting. The feasibility and the success of an application strongly depends on accurate estimations of the overall energy budgets, which are composed of several contributions.

Firstly, the power available from the energy transducers must be estimated to identify the main operating constraints for a given application. These assessments involve modelling energy transducers and also environmental surrounding conditions. More specifically, e.g. in the case of vibrational energy harvesters, the analysis of available input power requires to gather information about the vibrations such as amplitude, frequency spectrum, RMS, etc., as well as about the transducer such as theoretical/empirical model, mechanical and electrical properties, etc., in order to be able to predict the generated power. It is worth to mention that also the micropower management subsystem plays a key role in this process: the effectiveness in maximum power point tracking and the electrical conversion efficiency directly impact the power made available to the system. Ideally, an estimate of energy budget should account for both.

As a further necessary step, the extracted energy has to be stored inside the system, for use either in short or long term. For this purpose, models of energy storage devices have to be developed, including electrical data and physical characteristics. In order to predict the effectiveness of a novel energy storage solution, it is also necessary to model at a lower level electrochemical and physico-chemical characteristics as well as both materials and devices.

Finally, at system level, the produced or stored energy is consumed. The energy utilization process should account for the maximum possible efficiency. This is usually done along two main directions: circuit consumption optimisations and efficient switching between active, stand-by and sleep modes. Hardware characterisations play then an important role in defining the energy budget of an application, and representing the main data. At a higher level, application modelling involves combining the hardware consumption data to represent the actual behaviour and to make it compatible with available energy. Common techniques involve duty-cycling the main execution loops, or dynamic configuration of performance, accuracy depending on the currently available energy.

This report includes the contributions of ENABLES partners in the above-mentioned domains. The next section deals with modelling of vibrational energy transducers, whereas the following sections describe respectively the results obtained in modelling energy storage and system-level architectures.

4 Modelling vibrational energy

In the field of vibrational energy harvesting, given the variety of possible input vibrations, transducers, and electronic interfaces, it becomes important to assess in early phases of system design the corresponding power availability.

Electromechanical models based on lumped parameters, as shown in Figure 1, usually represent an effective trade-off between accuracy and complexity. This type of models can be easily translated into equivalent electromechanical circuits, which offer the possibility of joint simulations with power conversion circuits by using conventional and widely diffused software tools. However, given a particular transducer, analytical identification of model parameters is not immediate and may lead to unperfect matches with results from experimental characterisation due to the numerous degrees of freedom and involved parameters.

In this context, the ENABLES project contributed by developing models, software tools and experimental techniques for representing and assessing vibrational energy harvesters, with a focus on piezoelectric and electromagnetic transducers. Results in this respect are reported in the following subsections.

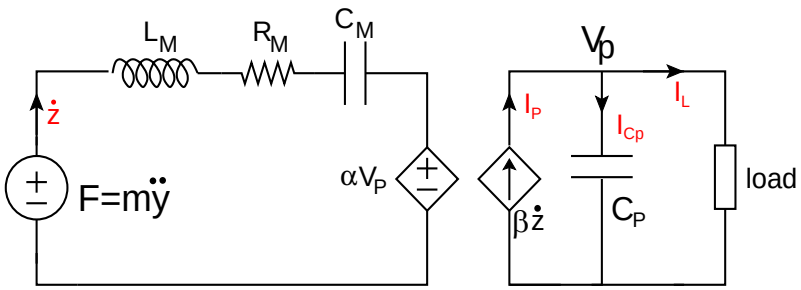

Figure 1. Equivalent electromechanical circuit of a piezoelectric transducer. $\dot{z}$ is the oscillation velocity, $\ddot{y}$ is the acceleration of input vibrations, m is the equivalent system inertial mass, α models the converse piezoelectric effect, β models the direct piezoelectric effect, L_M accounts for kinetic energy in the system, C_M accounts for elastic energy, R_M for mechanical losses, V_P and I_P are the voltage and the current generated by the transducer, respectively.

4.1 Modelling techniques for piezoelectric transducers and experimental identification of model parameters

An experimental test chain was developed and tested by the University of Bologna with the aim of identifying and characterising electricals model for piezoelectric transducers for energy harvesting. The type of transducers used in the experiment is the PPA (Piezo Protection Advantage), produced by Mide Technology, which encapsulates high-performance brittle piezo ceramics between copper-clad insulating materials. This family of transducers is characterised by sufficient mechanical robustness and less variability with respect to environmental variables, compared to the unsealed types. It is also easy to connect and quick to integrate into applications, thanks to the numerous holes for fixing and for mounting appropriate masses on its end. It is worth to highlight that the procedure presented herein has general validity and can be applied to most oscillating piezoelectric transducers.

Wires were soldered on the transducer to reach the electrodes on the encapsulated piezoelectric material. A suitable seismic mass was placed at its end, to tune its resonance frequency and to accentuate the gain peak. Through custom 3D printed supports, the transducer was fixed on the plate of a Tira S 51110 electrodynamic shaker. In the proposed setup, the shaker is configured to have horizontal displacement, i.e. with perpendicular motion with respect to the direction of the force of gravity.

Figure 2. A picture of the experimental setup, including a view of the electrodynamic shaker, the laser distance measurement sensors, the piezoelectric transducers with the 3D printed assembly structures.

In order to electromechanically characterize the structure, the setup of Figure 2 has been implemented. The blocks are highlighted in Figure 3. Harmonic oscillations of programmable amplitude and frequency are applied with a waveform generator. Two Keyence laser distance measurement sensors track in real-time respectively the motion of the base of the transducer and of the oscillating end, in order to provide by subtraction an effective way to assess the actual displacement of the transducer end with respect to the base. Multimeters and oscilloscopes are used to acquire relevant electrical quantities.

In a first set of measurements, the transducer terminals are shorted. The following quantities are acquired:

- amplitude of the sinusoid relative to the displacement detected by the laser pointed at the base of the shaker,
- amplitude of the sinusoid relative to the tip of the transducer,

- frequency of the sinusoidal stimulus in input,
- phase shift between the movement of the anchored end and movement of the transducer tip.

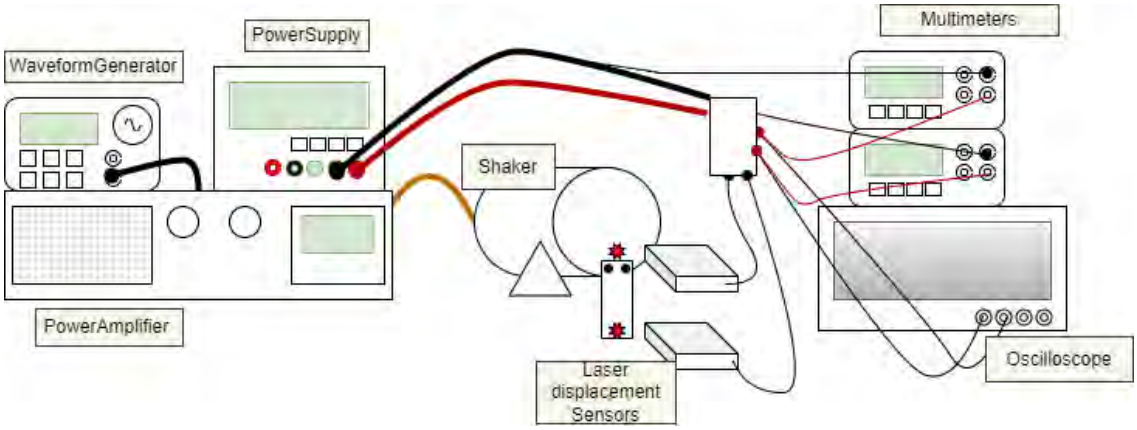

- **Figure 3. A sketch of the adopted experimental setup proposed for characterising piezoelectric energy harvesters**

Values of acceleration ranging between 0.2g and 0.3g were applied, where g = 9.81 m/s^2. By sweeping the vibration frequency, it is possible to identify the mechanical resonance frequency and the corresponding pulsation ω_m, where the maximum elongation occurs. Each normalized mechanical response of the transducer can be referred to an equivalent RLC admittance. In order to identify the corresponding parameters (Figure 1), a frequency sweep is performed, and we can define the quantity $\Delta\omega$ as the difference $(\omega_2 - \omega_1)$ between the two pulsations ω_1 and ω_2 at which the obtained oscillation velocity $\dot{z}$ is equal to $\frac{\dot{z}_{max}}{\sqrt{2}}$, where $\dot{z}_{max}$ is the maximum velocity, which is achieved at resonance. If we normalize with respect to the force corresponding to the input vibrations F, The parameters of the electromechanical equivalent circuit shown in Figure 1 can be identified: R_M is $\frac{1}{\dot{z}_{max}}$, L_M is $\frac{R_M}{\Delta\omega}$ and C_M is $\frac{1}{L_M\omega_m^2}$. The chosen range of amplitudes is coherent with the amplitudes of vibrations typically available in relevant application scenarios. The amplitude of tip motion remains limited so that it can be safely linearized.

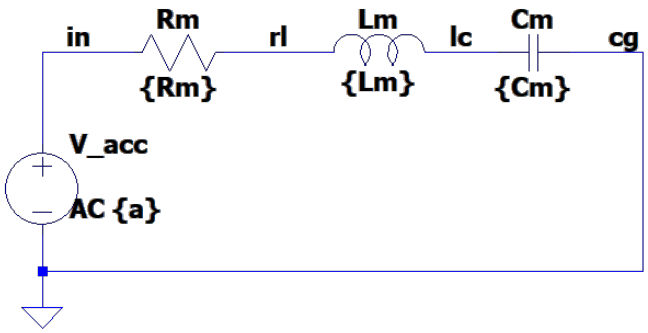

Figure 4. Simulated equivalent electromechanical circuit (shorted transducer)

The extracted equivalent electromechanical circuit (shorted transducer), see Figure 4, was then simulated with the LTSpice simulator to obtain the mechanical response. Figure 5 compares the experimental results obtained from measuring the actual displacement and by computing the

corresponding velocity, with the simulation results obtained with the equivalent electromechanical circuit with the identified parameters. A reasonable match of the curves can be observed, especially in proximity of the mechanical resonance frequency, although slight differences in the mechanic behaviour can be determined. It is worth to note the equivalent electromechanical circuit approximates the actual behaviour and is usually recognized in scientific literature as being more accurate in the near-resonance region.

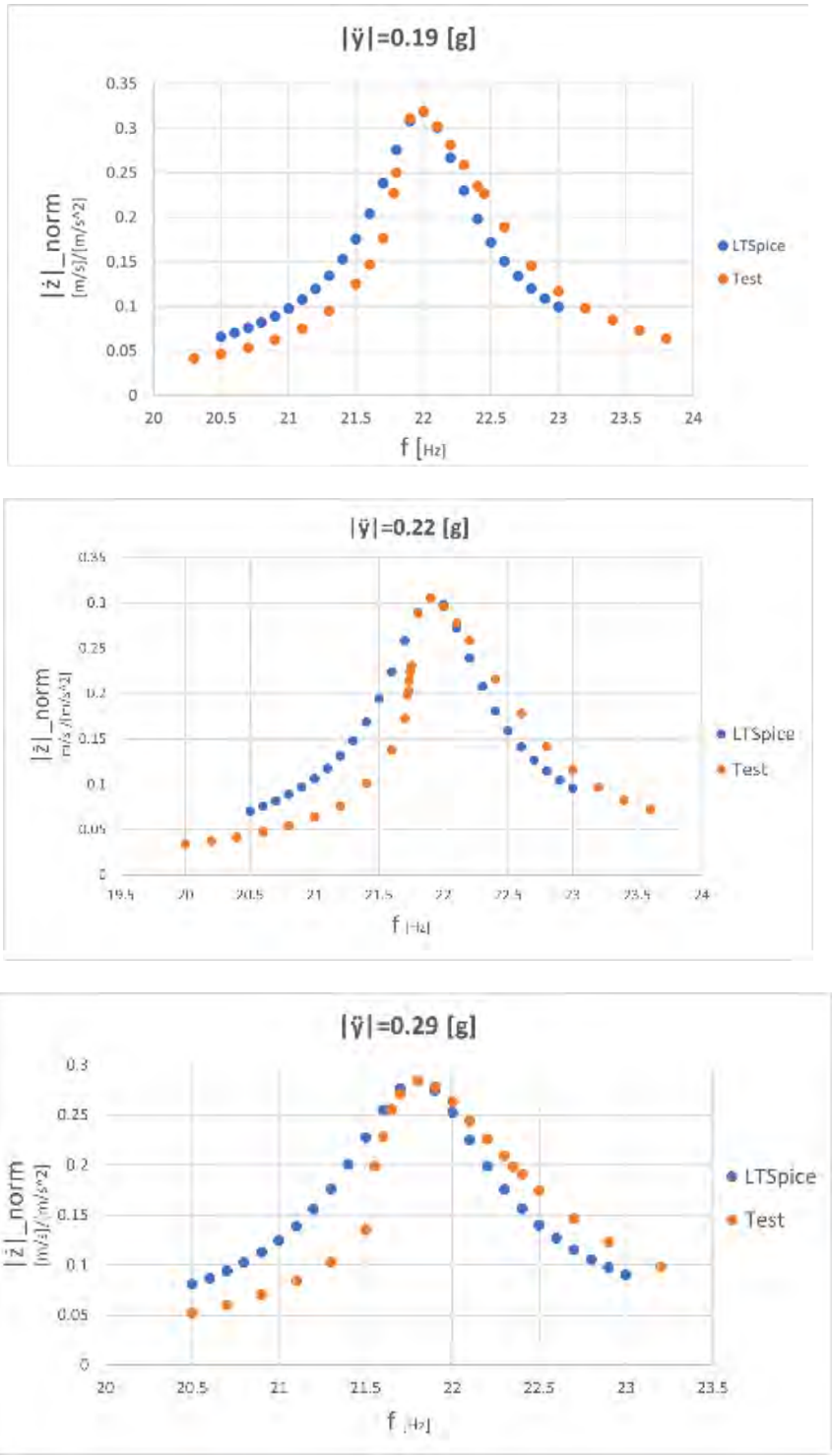

Figure 5. Comparison of measured and simulated data for the shorted Midé PPA-1011 piezoelectric transducer. Data are normalized with respect to the actual input vibration amplitude $\ddot{y}$ at every frequency, which was set respectively at amplitudes of 0.19g (top), 0.22g (middle), 0.29g (bottom).

The second set of measurements aims at measuring the short circuit current, by directly using a multimeter in current mode or by using a voltmeter and a shunt series resistor, whose value is negligible with respect to the transducer output impedance. The measurement procedure is the same as in the first set of measurements. All the mechanical (oscillation velocity, base acceleration, phase shift between the two motions) and electrical (output voltage/current in amplitude and phase) quantities are acquired. Figure 6 shows the dependency of all the short circuit current with the measured velocities $\dot{z}$. The relation between transducer's velocity and short circuit current remains linear across all frequencies and amplitudes of the input stimulus. This measurement allows the value of the coefficient β (as defined in Figure 1) that describes the direct piezoelectric effect to be determined.

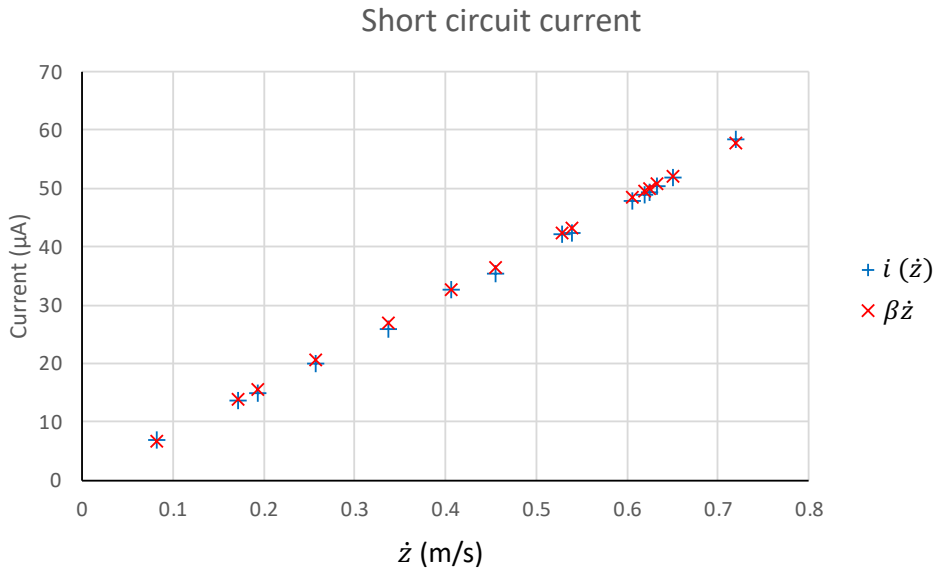

Figure 6. Comparison between (blue) measured current at different input velocities, (orange) linearized trend of the current, with slope and intercept' contributions, (green) linearized trend of the current with only slope's contribution, i.e. beta

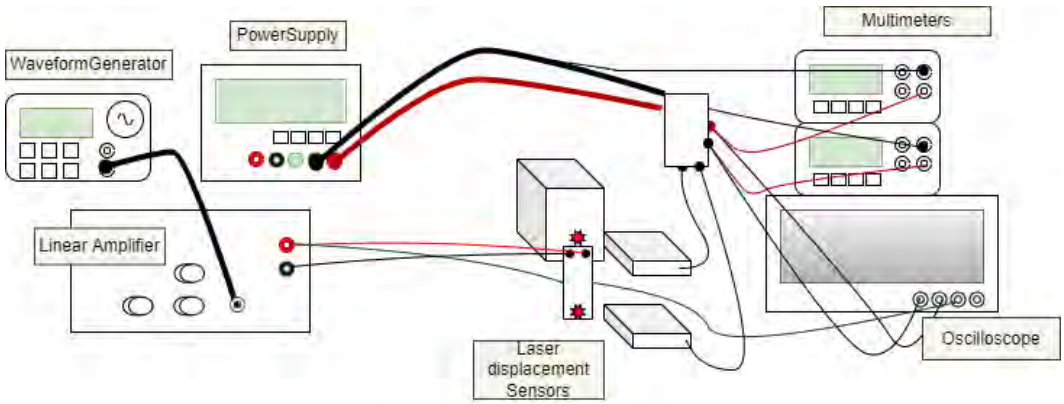

Figure 7. Experimental setup used to assess the converse piezoelectric effect.

The subsequent set of experiments has the purpose of determining α, i.e. the converse piezoelectric coefficient. The new experimental setup is depicted in Figure 7. The transducer is now anchored to a fixed mechanical support and is stimulated electrically by a signal produced by a waveform generator and a voltage amplifier. Since a voltage generator is connected to the transducer, the effects of the capacitance C_P are cancelled and the mechanical behavior is the same as in the short circuit condition.

As it can be observed in Figure 5, the resonance frequency of the bare mechanical system shows a dependency on the amplitude of applied motion, and similarly it depends on the amplitude of applied voltage V_P in this configuration, which from a mechanical point of view applies a force αV_P. With the use of an oscilloscope, it is possible to identify for which applied input voltage amplitude, the resonance frequency (i.e. the frequency at which the tip displacement is 90° out of phase with respect to the forcing voltage) matches the ones obtained previously. Maintaining the desired resonance frequency, once the amplitude to be applied is defined, a frequency sweep at that amplitude is applied, and the mechanical displacements are measured with laser sensors and normalized with respect to V_p. At this point, the previously used expressions are used to compute new parameters of the equivalent circuit R'_M, C'_M, L'_M to fit the new curve. Since the measurements are normalized with respect to V_p (it can be seen in the equivalent circuit in Figure 1 that the generator αV_P has the same units of the force generator), it is expected that the new parameters are scaled by a factor α with respect to those identified in the previous step (i.e.). This is also verified experimentally. For this reason, α is identified as the average of the ratios $\frac{C'_M}{C_M}, \frac{R_M}{R'_M}, \frac{L_M}{L'_M}$. In this set of measurements, the reported results involve a peak-to-peak voltage input equal to 149V. The resonance frequency is 21.9 Hz, as previously obtained for an amplitude of input accelerations between 0.2g and 0.25g.

Figure 8 reports the results of the normalized measurements compared with the values derived by the equivalent model.

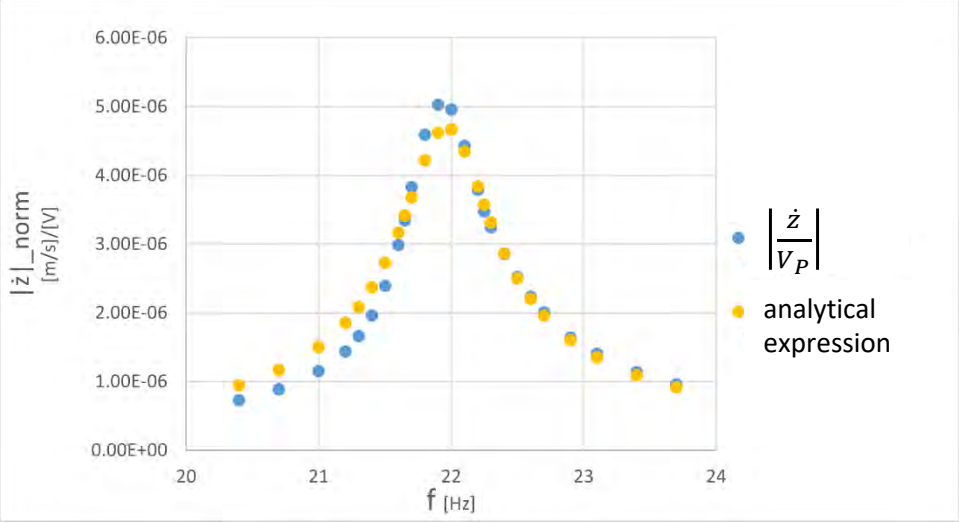

Figure 8. Comparison between normalized experimental transducer's velocity obtained with 149V peak-to-peak input voltage and analytical response of the equivalent circuit obtained using the extracted α, R_M, C_M, L_M parameters.

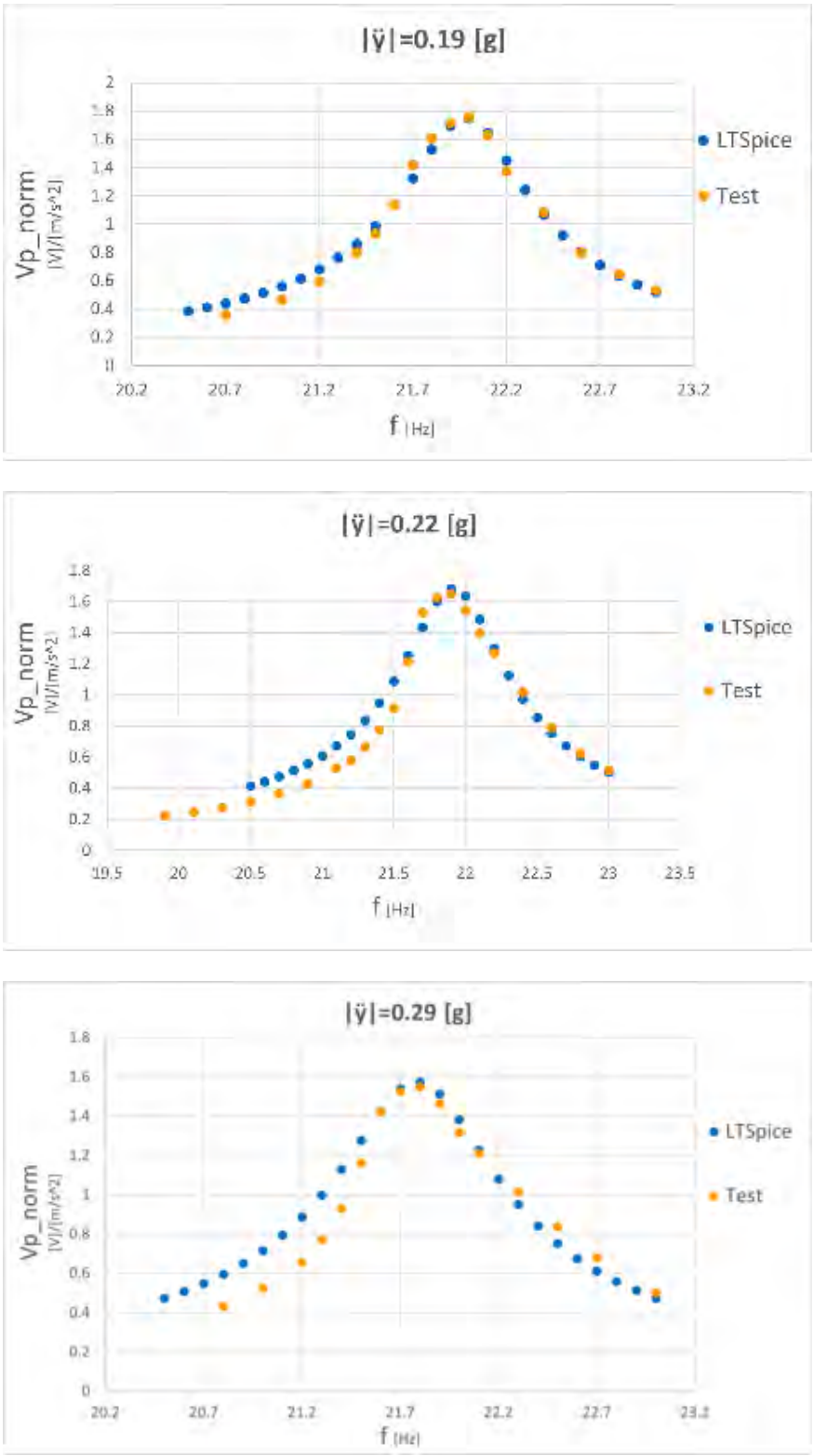

Figure 9. Comparison between experimental values (orange) and data obtained from SPICE simulation of extracted equivalent circuits (blue) at three different amplitudes of input acceleration, 0.19g (top), 0.22g (center), 0.29g (bottom).

Finally, to determine the value intrinsic capacitance of the piezoelectric transducer, i.e. C_p in Figure 1, it is possible to use an impedance analyzer, by setting a frequency far from the resonance evaluated earlier, so that mechanical effects become negligible.

At this stage, the model is complete and can be used to assess the behavior of the transducer in proximity of its resonance frequency. Figure 9 shows a comparison of the voltage across a $100\ M\Omega$ resistor obtained simulating the whole equivalent circuit at three different amplitude of input acceleration using LTSpice, and the voltage across a real $100\ M\Omega$ resistor measured experimentally in a real setup, show a good match, particularly in the near-resonance region. The obtained electromechanical circuit can be used in a circuit simulator jointly with power conversion circuits to assess the performance of the system.

4.2 Vibration Energy Harvesting On-line Simulation tools

In order to provide a tool for testing and assessing vibrational energy transducers, the ENABLES project has developed online simulation tools, which are accessible on the ENABLES website at the following URL: http://www.enables-project.eu/virtual-access-data/va-perugia. More specifically, as shown in Figure 10, two simulation tools have been developed:

- Vibration Energy Harvesting system independent from conversion technology type
- Piezoelectric Energy Harvesting based on a cantilever beam.

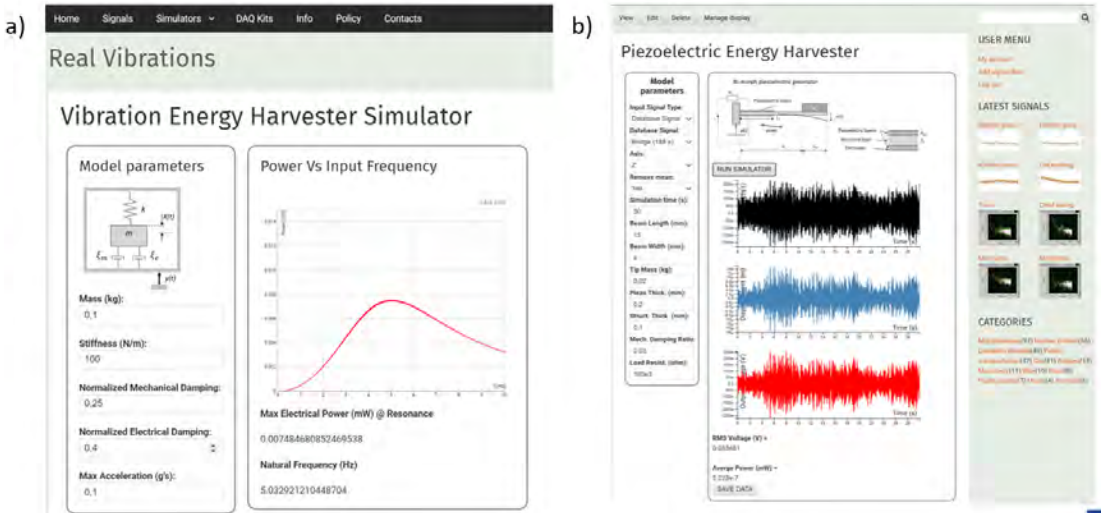

Figure 10. Webpage screenshots of online simulators of a) General Vibration Energy Harvester and b) Piezoelectric vibration energy harvester based on a cantilever beam.

These simulators have been developed by the University of Perugia in collaboration with the University of Southampton and are based on numerical integration of dynamic stochastic differential equations of the lumped 1-DOF theoretical models of the systems. The numerical integration is coded by JavaScript based on predictor-corrector algorithm and the input vibration signal can be selected from those available in the real vibration database or just ad sinusoidal wave. The calculations are performed in the user machine that has loaded the tool webpage. All the detailed description of the theoretical modelling are detailed in the EnABLES deliverable D5.4.

The results obtained with an electromagnetic vibration energy harvester simulator, which is still under testing and is not yet fully released on the ENABLES website, are shown in the following Figure 11.

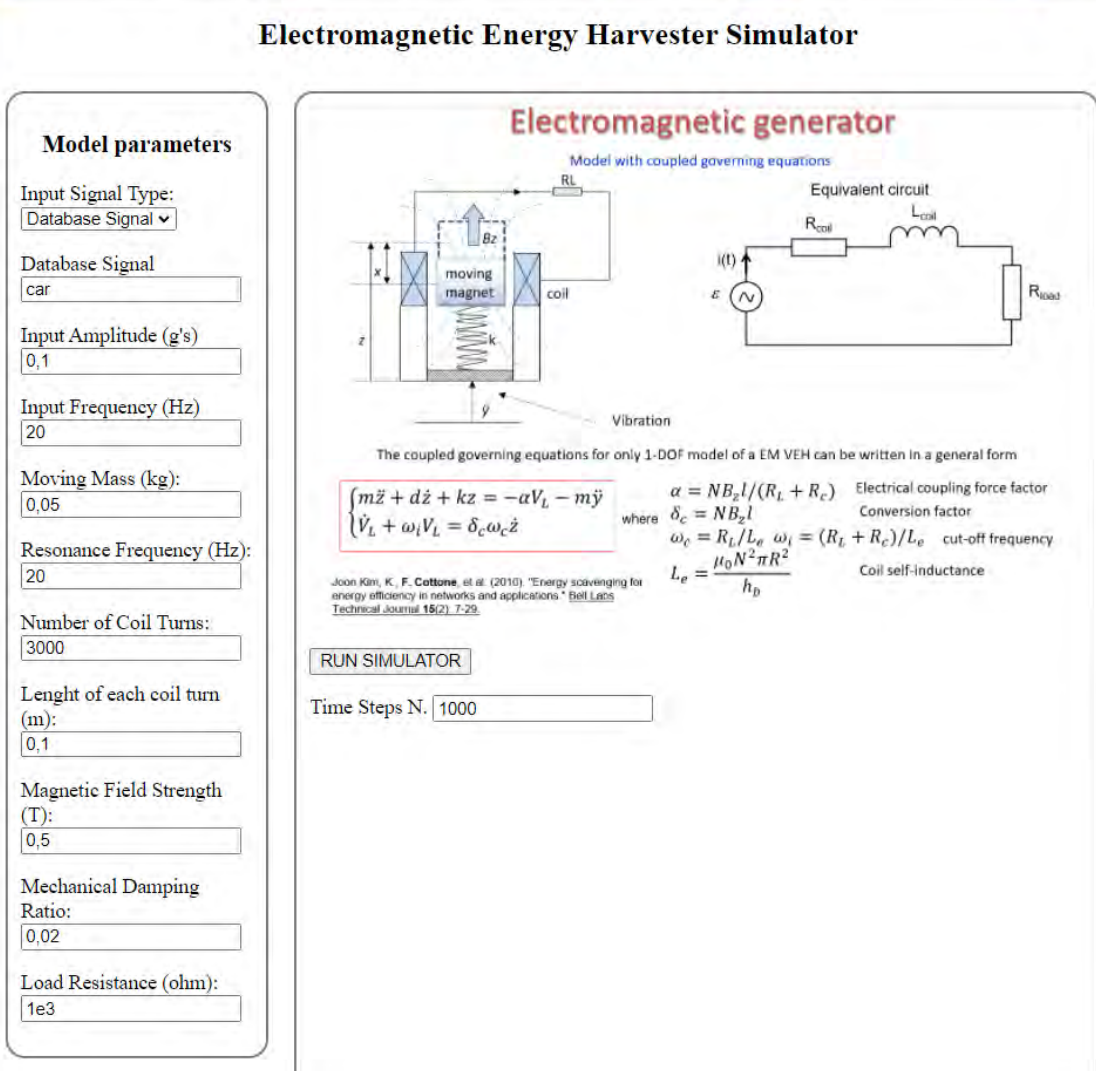

Figure 11 . Preview of the electromagnetic Vibration Energy Harvester Simulator

The main model is based on oscillating mass *m* integrated with permanent NdFeB magnets that generate a magnetic field *B* with flux linked through a coil. The electromotive force *V* generated by the flux change enters as damping term in the dynamical coupled equations: Newton equation and Kirchhoff equation. The inertial mass motion *Z* and the output voltage *V* are therefore calculated with same approach described in ENABLES deliverable D5.4 of the numerical integration of the coupled equations illustrated in Figure 11.

5 System-level energy modelling

Once energy transducers are properly characterized and the available power can be determined, in order to ensure the success of an application based on energy harvesting it is essential to be aware of the energy requirements of the electronic systems that should be powered. In this phase, trade-offs between performance, activation duty-cycle are likely to be necessary. Knowledge about energy requirements becomes then essential, also in the perspective of optimising the application behaviour. It is then relevant to assist designers with tools and set of data that ease the design and sizing of the application also from the energy perspective.

In this section the further developments in open-source system level simulation tools created so far (initially described in ENABLES deliverable D5.4) are outlined along with their initial usage in EnABLES TAs and another EU project (ReCO2ST). Moreover, experimental energy characterisation techniques on existing nodes are reported.

5.1 System-level simulation tools

A system simulation model (with associated GUI) can greatly assist 2 potential stakeholder groups:

(i) For developers of parts to simulate the behaviour of combinations of components (transducer, PMIC, passives, storage device) under different operating conditions and control schemes. In particular, models that accurately predict the load power profile and overall system efficiency and demonstrate the system level trade-offs (e.g. peak power versus effective bandwidth for vibrational devices, energy density versus operational voltage, charge cycle degradation and leakage current for storage devices)

(ii) For installers to help selection and sizing of components to meet a particular application need. Conversely, an assessment can be undertaken to see if a given combination of components can meet the system requirements.

As described in ENABLES deliverable 'D5.4 – 1st pass simulation tool', EnABLES partner Tyndall had previously developed 'ROWBUST', an early version of such a tool for both stakeholder groups but primarily targeted at helping users with no expertise in energy harvesting and IoT devices (e.g. wireless sensors). Since the Tyndall has developed a derivative simulation model under the EU project ReCO2ST where it was used to understand and optimise the power consumption and battery life of wireless sensors retrofitted in commercial buildings. The results of these efforts were presented at 2 conferences:

(i) SensorComm 2020 The Fourteenth International Conference on Sensor Technologies and Applications, *Towards Autonomous Smart Sensing Systems* https://www.iaria.org/conferences2020/filesSENSORCOMM20/10003_sensorcomm.pdf

(ii) The Advanced Building Skins Conference 2020 (ABS2020) and its associated journal. *'Sensor deployment to support the integrated energy management system in residential buildings in ReCO2ST'* https://zenodo.org/record/5569124#.YWgGuLjMI2w

A high-level summary of the outputs was also presented the EnABLES webinar on 25th Feb 2021 on WSN device power consumption simulation tools (Figure 12).

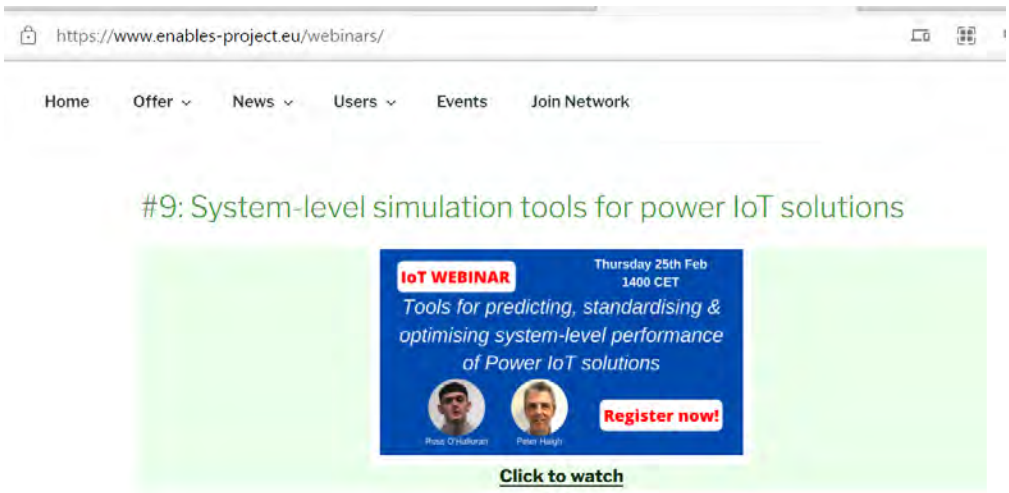

Figure 12. Screenshot of the ENABLES website with a link to the delivered webinar on simulation tools for assessing power consumption. The webinar is available online at https://www.youtube.com/watch?v=efZ8_p1-6u4

A summary of the material was also presented at a PSMA webinar on ‘Powering & Retrofitting IoT Devices for Industry 4.0’ as an example of the synergies from various projects to deliver impactful simulation tools to academic and industrial partners (Figure 13).

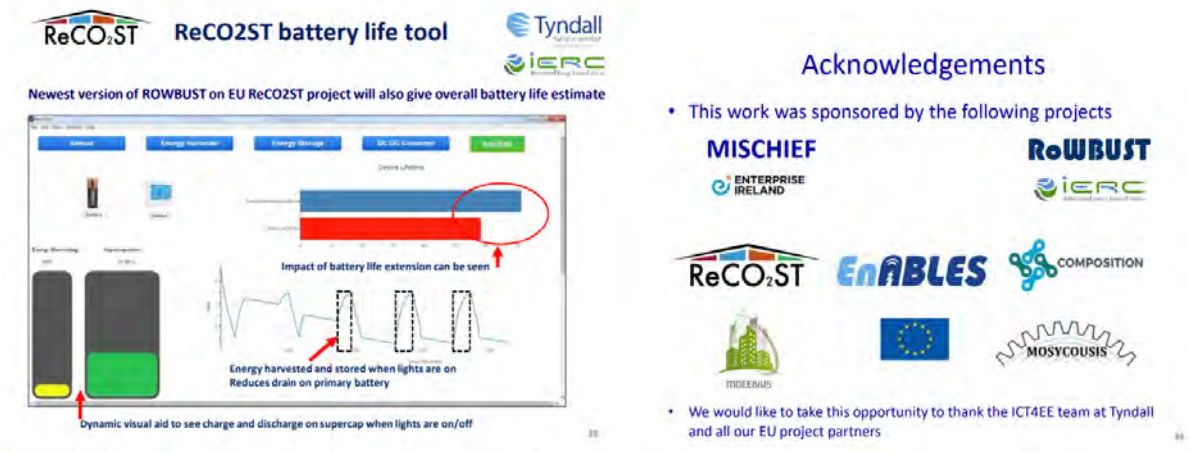

Figure 13. Summary of the material presented at the PSMA webinar of ‘Powering & Retrofitting IoT Devices for Industry 4.0’

Knowledge and experience gained in developing this tool is currently being used in a number of EnABLES TA, most notably #158 with the University of Ulster (UU). The tool will help UU understand the trade-offs between algorithm complexity (and its ability to self-repair a network over a long time span) versus power consumption of the algorithm/processor used. This can also be used to optimize microprocessor selection and determine feasibility and sizing for energy harvesting components.

A summary of the work to date on this TA was presented at the forthcoming PSMA Energy Harvesting industry session at international power electronics conference APEC2022 (along with other EnABLES use cases). Some screen shots are shown in Figure 14.

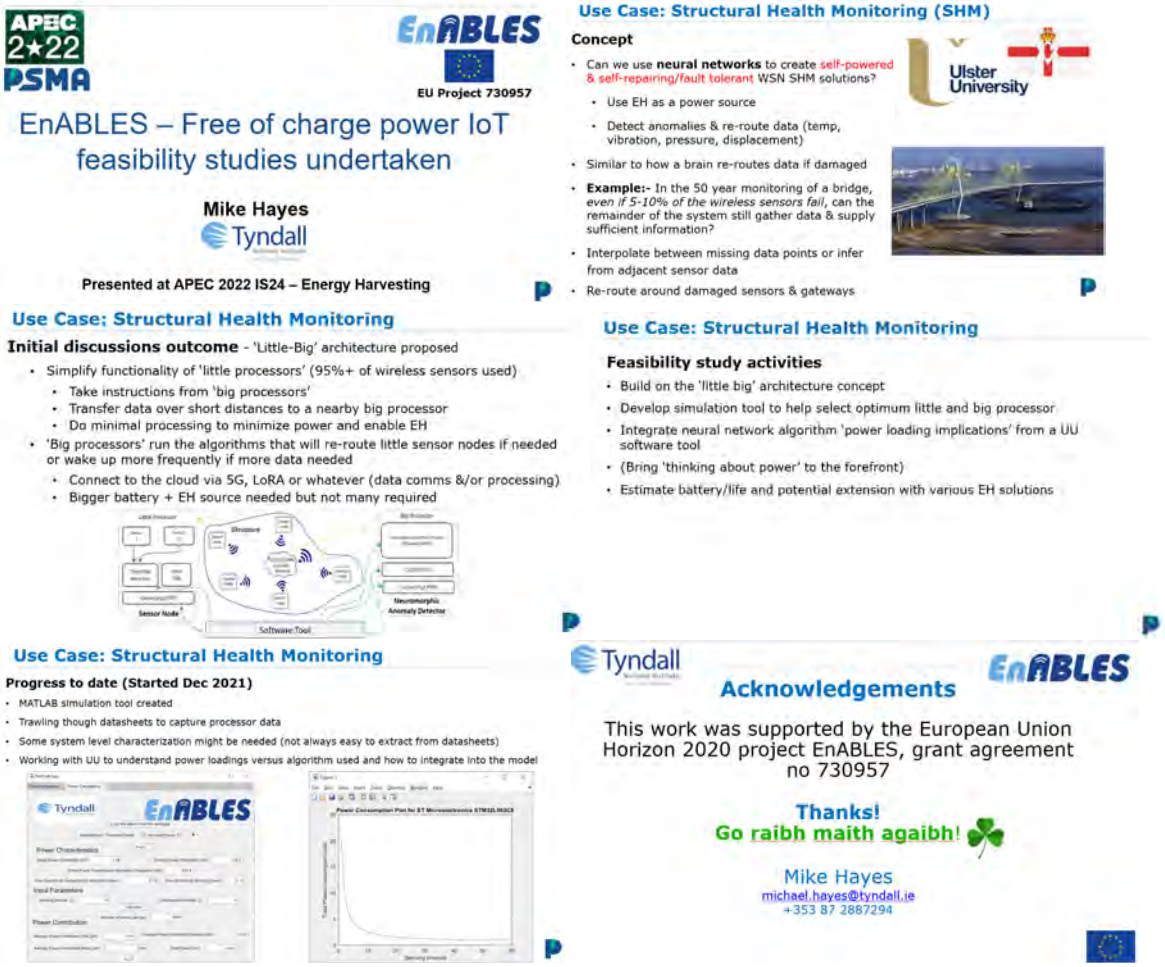

Figure 14. Summary of the work that will be presented at forthcoming PSMA Energy Harvesting industry session at international power electronics conference APEC2022

There are also plans for this simulation tool to be used in a recently approved TA (#161) with UK SME MDDS. The battery life of wireless sensors used for structural health monitoring of aircraft can be predicted and the impact of the selection of various combinations of components in different configurations can be assessed.

5.2 Energy models for easy characterization of configurable IoT nodes with energy harvesting capabilities

As described in previous ENABLES deliverable D5.4, this activity carried out by the University of Bologna relates to the development of a model of the power consumption of a family of IoT nodes with common characteristics (sensor capabilities, wireless transceivers, communication protocols, control/elaboration hardware, backup storage, actuators) and energy sources to evaluate the overall

energy budget of the system. Goal of the analysis is to identify the feasible operative conditions which make the nodes autonomous or self-sustainable, i.e. in which the average harvested energy $E_{av,HARV}$ is greater than the average energy consumed by the node $E_{av,SYS}$:

$$E_{av,HARV} \geq E_{av,SYS}.$$

Considering an integration reference period T_{REF}, since the power management system keeps the supply voltage constant, the previous formula is expressed in terms of charge balance in which Q_{av} is calculated as the node average current consumption times the reference period T_{REF}:

$$Q_{av,HARV} \geq Q_{av,SYS}.$$

$Q_{av,SYS}$ is made up of different contributions that can be present or not depending on the node type (sensor or actuator), on the node communication mode (Beaconing or Request/Response) and on the node phase (stand-by or data communication phase):

$$Q_{av,SYS} = Q_{av,SYS\_MOT} + Q_{av\_SB} + Q_{av\_COMM}$$

where Q_{av,SYS_MOT} is the charge consumption for actuation, Q_{av_SB} the charge consumption during the stand-by phase and Q_{av_COMM} the charge consumption during the data communication phase.

In D5.4 the proposed model was applied to nodes with diversified features and the effectiveness of the addition of a Wake-up Radio (WuR) was considered since it eliminates the overhead in communication protocol caused by synchronization procedure normally necessary during the stand-by phases between two subsequent node activations.

To further investigate the advantages in terms of reduction of the average energy consumed by the node ($E_{av,SYS}$) offered when using WuRs, in the last period we designed and tested a prototype working in the nanowatt regime. The experimental results of the WuR characterization were substituted in the model described in D5.4 to analyse the condition for nodes with different features to be autonomous.

WuR prototype. The WuR prototype block diagram is shown in Figure 15. The always on Analog-Front-End (AFE) is clockless, i.e., it does not need an oscillator, while the baseband logic requires a clock to sample the incoming data. This allows the WuR to operate in two phases. During phase 1, the baseband logic is off whereas the AFE is active. Phase 2 starts upon recognition of the first 0-to-1 transition of the message, occurring at the first transition of the AFE output signal Din: the baseband logic is turned on, the gated oscillator starts running and the incoming bitstream is compared with the stored codeword. This approach allows reduction of the power consumption of the node if the specific application is characterized by long idle periods, since the baseband logic is off most of the time.

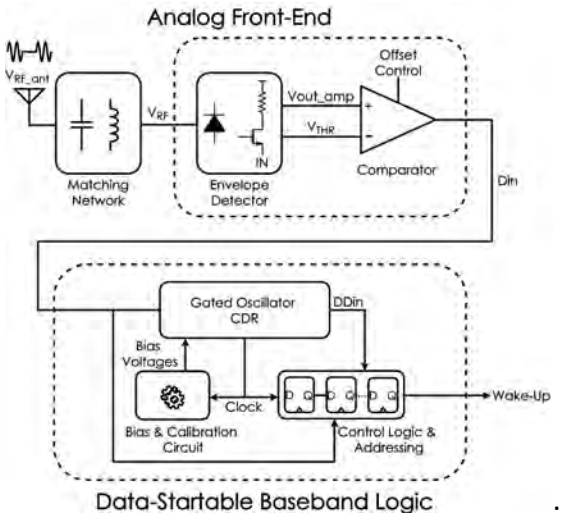

Figure 15. WuR block diagram (from M. D'Addato et al, "A Gated Oscillator Clock and Data Recovery Circuit for Nanowatt Wake-Up and Data Receivers" Electronics, 2021)

The AFE is composed of an Envelope Detector, which simultaneously extracts the envelope of the incoming OOK signal and amplifies it at baseband, a comparator with variable threshold to digitize the extracted envelope, and a reference current generator to provide bias currents for both the ED and the comparator. All transistors operate in subthreshold region with 0.6 V power supply. The baseband logic includes a Gated Oscillator Clock and Data Recovery block (GO-CDR), which provides a clock signal to the control logic (CL) that samples on positive edges delayed version of the input data (DDin) and generates the wake-up signal upon reception of the correct codeword. The GO-CDR guarantees the phase alignment between received data and clock at each data (Din) transition.

The prototype has been designed using a STMicroelectronics 90 nm BCD process. The overall power consumption is lower than 13 nW during phase 1 and increases to 17 nW during phase 2 at 1-kbps data rate, with a sensitivity, including the external matching network, of -43 dBm at 868 MHz.

Sustainability analysis of IoT nodes integrating the WuR. We studied the Indoor Wireless Sensor and Actuator Network (WSAN) described in D5.4 and shown in Figure 16 for clearness.

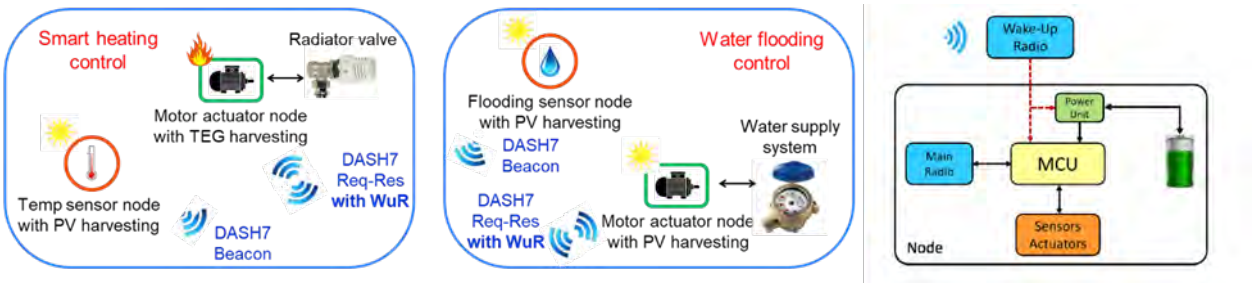

Figure 16. ***WSAN with low power communication protocol stack and Wake-up Radio capability***

As shown in Figure 16, the nanowatt WuR prototype has been integrated in the motor actuator nodes with TEG (for smart heating control) or PV (for water flooding control) harvesting: these nodes are

configured in request/response mode where the use of a low-power WuR allows to eliminate the power consumption caused by synchronization procedure normally necessary during the stand-by phases between two subsequent activations of the node. Due to the nanowatt range of prototype WuR power consumption, we expect to reduce the stand-by charge consumption (Q_{av_SB}) and the communication charge consumption (Q_{av_COMM}) compared to the implementations analysed in D5.4. Moreover, we performed an optimization in terms of power consumption also in the protocol stack and in the sleep state of the microcontroller of the actuator node, which led us to further lower the energy consumption of the whole system (compared to the same node in D5.4).

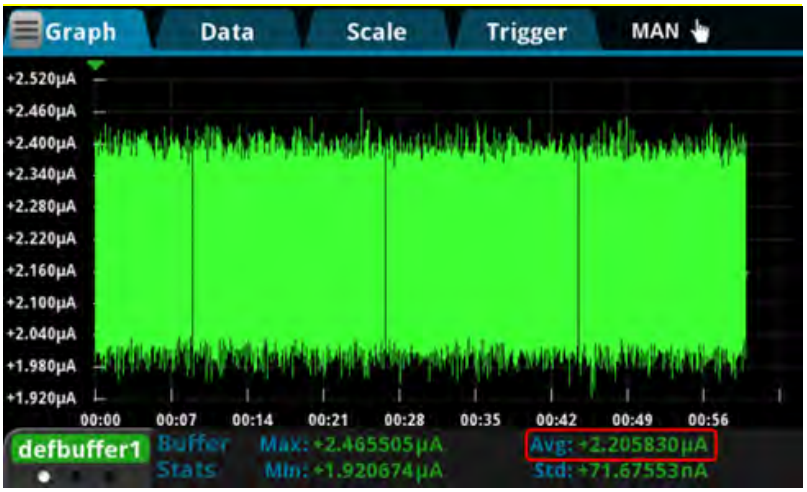

Figure 17. ***Current consumption profile of the actuator node with WuR in stand-by phase. A 2.2 µA average current is computed in a 60 s reference period as highlighted in red***

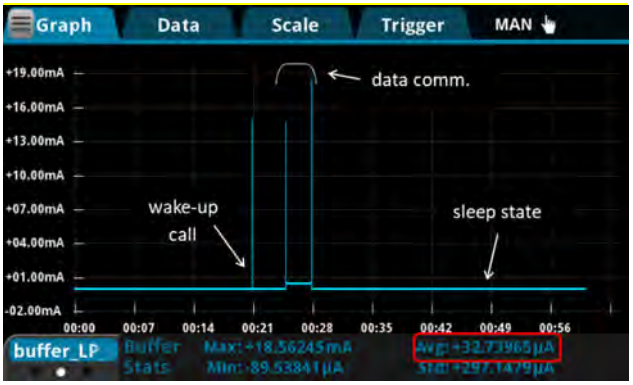

Figure 18. ***Power consumption of the actuator node with WuR when a wake-up call and data communication is performed (communication phase). A 32.7 µA average current is computed in a 60 s reference period as highlighted in red.***

Figures 17 and 18 show the current profiles of the node in stand-by and communication phases. Considering T_{REF} = 60 s as integration reference period, the node average current consumption in sleep state (stand-by phase) is reduced to 2.2 µA from the 6 µA measured with the non-optimized node used in D5.4, whereas the average current consumption during a communication phase, i.e during T_{REF} one wake-up call and data communication is performed, is about 32.7 µA (instead of 160 µA). Table I summarizes these numerical results.

Communication mode	Node average current consumption in T_{REF} = 60 s	
	One data comm. in T_{REF} (I_{av_COMM})	No data comm. in T_{REF} (I_{av_SB})
Request/Response	32.7 µA	2.2 µA

Table I. M*easured average current consumption of the actuator optimized node with WuR*

Starting from these current consumption measurements, we applied the energy model described above (and also previously described in deliverable D5.4) to verify the performances of the motor actuator optimized nodes with TEG or PV harvesting and to calculate the minimum time between subsequent motor activations to have the node self-sustainable. The results are shown in Table II.

Node type	Light [lux]	Q_{av_HARV} PV [mC]	Q_{av_HARV} TEG [mC]	Q_{av_SB} [mC]	Q_{av_COMM} [mC]	$Q_{av\_SYS\_MOT}$ (10 %) [mC]	Self-sustainability
PV harvesting motor actuator node with WuR in stand-by phase	115	1.08	/	0.13	/	/	✓
TEG harvesting motor actuator node with WuR in comm. phase and motor on	/	/	13.2		1.96	48	3.8 min

Table II. S*ustainability analysis for motor actuator node with TEG/PV harvesting and WuR. Charges are calculated as average current times the reference period T_{REF}= 60 s*

In water flooding control applications, the brushed DC motor must close the valve connected to the water supply system in case a water flooding alarm is sent by the flooding sensor nodes. The actuator node operates therefore always in stand-by phase except a single communication phase when the command to close the valve is sent from the coordinator.

To evaluate the self-sustainability of the node, let us find the minimum period $n*T_{REF}$ during which $Q_{AV,HARV} > 0$ which guarantees the node is properly working all the day ($24*60*T_{REF}$).

$$Q_{av,HARV} * n \geq Q_{av,SB} * 24 * 60.$$

Using the values in Table II, it can be found that the actuator node with PV harvesting is self-sustainable even with a typical low-level home daylight intensity (115 lux corresponds to a charge of 1.08 mC in one reference period T_{REF} = 60 s) for only 173 minutes, i.e about 3 hours.

In smart heating control the average charge absorbed by the node $Q_{av,SYS}$ must take into account also the current consumption due to the communication with the coordinator and the current consumption supplied to the motor (Q_{av,SYS_MOT}) which has to be moved frequently to track the desired temperature.

To evaluate the condition for self-sustainability of the node with TEG harvesting, we calculate the minimum time ($n*T_{REF}$) between two subsequent motor activations (assuming each activation performs a movement equal to a 10 % of the full valve range) to have the node self-sustainable:

$$Q_{av,HARV} \geq Q_{av,SYS}$$

$$Q_{av,HARV}*n \geq Q_{av,SYS\_MOT} + Q_{av\_SB}*(n-1) + Q_{av\_COMM}$$

where $Q_{av,SYS}$ is computed by summing the charge contribution of (n-1) reference periods where the node is stand-by phase and one period where the command to close/open the valve is sent from the coordinator and the motor is actuated (i.e the node is in communication and actuation phase). Using the values in Table II, it is found that the valve can be moved as frequently as every 3.8 minutes.

Thanks to the hardware/firmware optimizations and the use of the new nanowatt WuR, this time interval is 15% lower than the one reported in D5.4 in the same conditions. Analysing more deeply the charge contributions in the table, it can be observed that the average charges consumed by the node in stand-by phase (Q_{av_SB}) and in communication phase (Q_{av_COMM}) are much lower than the previous implementation (of about 63% and 80% respectively), but considering the minimum time between subsequent motor activations, the advantage is less clear because the charge consumed by the running motor is predominant ($Q_{av\_SYS\_MOT}$ = 48 mC).

6 Modelling and characterization of energy Storage

Models and methods for implementing innovative storage devices play an important role in the progress of IoT. This section describes the development and the manufacturing techniques for implementing flexible and complements the previous results achieved in vibration energy harvesting and system-level energy modeling. The data obtained during the development and construction of printed batteries and transistors is needed as a basis for future calculations of more complex printed devices. With the key parameters obtained from the printed electrode/transistor combinations, predictions for future systems can be made and realized.

6.1 Development and manufacturing techniques of flexible energy storage systems

The KIT contribution to ENABLES deliverable D5.5 includes the investigation of development and manufacturing techniques of flexible energy storage systems and their characterization. On the one hand this includes the development of novel materials for energy storage devices, on the other hand the transfer of applicable materials to suitable manufacturing processes. The development of novel electrode materials, mostly based on the high-entropy approach, will be described in the final deliverable D5.6. Here, the results of the preparation approach for flexible energy storage devices with known electrode materials will be presented.

The focus of this work has been set to printing methods, since these additive manufacturing techniques enable a stepwise manufacturing approach, allow the utilization of a broad range of different materials and reduce waste production, which is inherent in subtractive techniques. More precisely, ink-jet printing and plotting technologies have been investigated for their applicability to print electrodes for Li-based battery technologies. Li-ion batteries are the most prominent battery types on the consumer market, therefore a transfer from macroscale batteries, like in cars or portable electric devices, towards mini/microscale sizes that can be used in IoT devices is necessary in order to store energy supplied, e.g., by energy harvesters directly on site. In this regard, known electrode materials have been taken, processed to form an ink-jet printable ink, printed on a current collector and tested against different counter electrodes in a laboratory scale Li-ion battery.

As active material, pure Si was taken as electrode material, since it is considered to be a promising higher energy/power alternative to graphite anodes. Indeed, the theoretical gravimetric capacity of Si is about 9-10 times larger than that of graphite (ca. 3500-3700 mAh/g vs. ca. 370 mAh/g), and first anodes containing a mixture of Si and graphite to combine capacity and fast lithiation kinetics are close to commercialization.

In order to print Si as electrode material, an ink-jet printable ink had to be prepared. We were able to publish this research in the peer-reviewed journal Batteries & Supercaps (Impact Factor 7.1)[2]. We were able to develop two different printable aqueous inks (Figure 19 a), one containing only Si with a mixture of a binder polymer (PVA), water and conductive carbon (C65), and the other ink containing carbon

[2] P. A. Sukkurji, I. Issac, S. A. Singaraju, *et al.*, "Tailored Silicon/Carbon Compounds for Printed Li–Ion Anodes", *Batter. Supercaps* **3**, (2020), 713–720, 10.1002/batt.202000052

coated Si with PVA, water and conductive carbon. The coating of Si with carbon led to a facilitation of the printing process and enabled to print much smoother surfaces. Additionally, this carbon increases the electronic conductivity of the active material compared to insulating Si. The details about ink preparation can be found in our publication in Batteries & Supercaps[2].

The idea to coat Si with C derived from the observation that pure Si inks often agglomerate easily. Agglomerations can have a negative impact on the printing process, e.g. by clogging the printing nozzles. Therefore, we developed a technique to prevent the agglomeration. Particle agglomeration is often a result of large surface energies, hence coating the surface with a material resulting in a different zeta potential can lead to a different agglomeration behavior. By coating Si with carbon we could detect a much less pronounced agglomeration and the inks were better suited for printing processes.

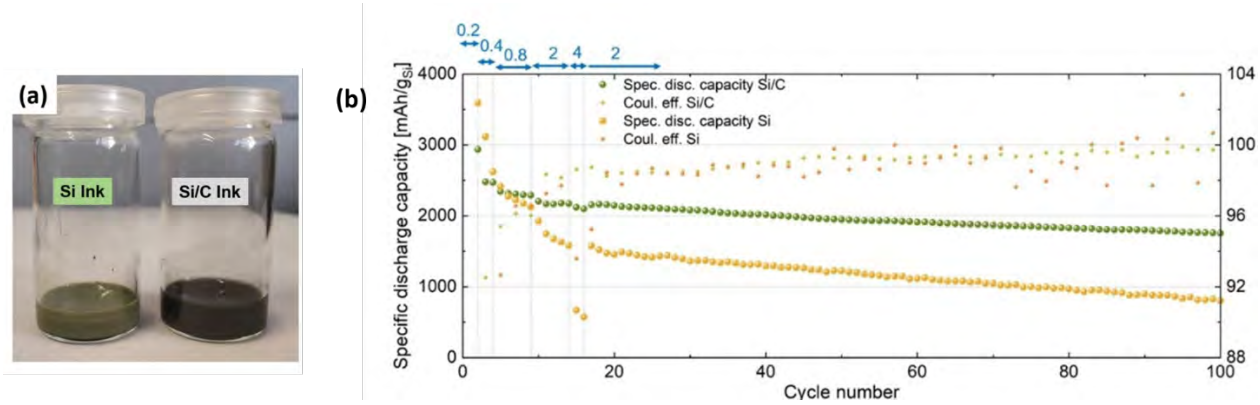

Figure 19. a) different inks prepared of raw Si and carbon coated Si[2]. b) Gravimetric capacity of the printed Si electrodes[2].

Exploiting plotting techniques, we prepared flexible electrodes out of both inks that could deliver large capacities over more than 100 cycles, when cycled against Li as counter electrode and using a standard liquid electrolyte. Clearly, the carbon coated Si showed improved electrochemical performance, particularly enhanced stability, compared to pure Si electrodes (Figure 19 b).

In addition, the printed Si electrode was tested in a full cell, using layered NCM ($Li(NiCoMn)O_2$) as cathode active material. The full cell showed reversible cycling, which makes it capable to supply a potential that is sufficient to power a printed transistor. Printed transistors are the backbone of every flexible IoT device, and needs a certain operation voltage in order to switch on and off. It was shown that our printed Si / NCM full cell could be used to switch a printed transistor on and off (see Figure 20), leading to the conclusion that such systems are in principle suitable for the power supply of flexible IoT devices.

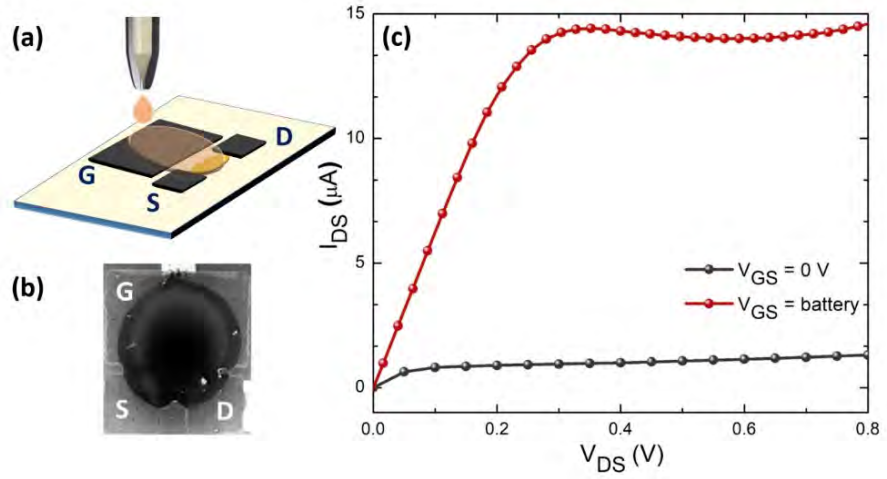

Figure 20. a) Preparation of an in-plane printed transistor that should be switched on and of using the printed flexible Si/C electrode as anode in a Si/C / NCM battery. S = Source, D = Drain, G = Gate[2]; b) Optical microscope image of the prepared printed transistor; c) Output curve of a printed transistor, switched on and off using a Li-ion battery full-cell with the printed Si as anode. The battery was connected to the Source and the Gate in order to switch the transistor on and off[2].

7 Conclusions

This deliverable showcased the progresses of the ENABLES project in the field of modelling and simulation tools at different levels related to energy harvesting systems. The work covered topics ranging from modelling and characterisation of energy transducers to system-level energy budgeting. Moreover, modelling and characterisation of innovative energy storage devices were presented to complement the discussion. The obtained data represent a useful basis for predictions of future systems.

As ENABLES pursued a holistic approach in pursuing developments in powering the Internet-of-Things, the developed models represent an effective way to close the loop. Firstly, techniques for identifying equivalent circuit models of commercially available piezoelectric transducers were proposed. This allows joint simulation of non-linear energy conversion circuits and being able to apply custom vibration sets at the input as well, for early-stage predictions of energy availability. Complementarily, web-based tools were developed and made available to the public for performing online simulations of vibrational energy transducers. However, effective applications can be implemented only if an energy-aware design is carried out since the initial phases. For this purpose, simulations tools and energy models of IoT devices were developed and summarised in this report. Knowledge of power and energy in the different operating phases of a system is necessary to ensure positive energy budgets.